INTERNATIONAL JOURNAL FOR NUMERICAL METHODS IN ENGINEERING
Int. J. Numer. Meth. Engng 2005; **64**:1509–1528
Published online 29 July 2005 in Wiley InterScience (www.interscience.wiley.com). DOI: 10.1002/nme.1411

An incremental 2D constitutive model accounting for linear viscoelasticity and damage development in short fibre composites

J. Varna[1] and M. Oldenbo[2,*,†]

[1]*Division of Polymer Engineering, Luleå University of Technology, SE-971 87 Luleå, Sweden*
[2]*Volvo Car Corporation, Exterior Engineering, Dept 93610, PV3C2, SE-405 31 Göteborg, Sweden*

SUMMARY

A model accounting for linear viscoelasticity and microdamage evolution in short fibre composites is described. An incremental 2D formulation suitable for FE-simulation is derived and implemented in FE-solver ABAQUS. The implemented subroutine allows for simulation close to the final failure of the material. The formulation and subroutine is validated with analytical results and experimental data in a tensile test with constant strain rate using sheet moulding compound composites. FE-simulation of a four-point bending test is performed using shell elements. The result is compared with linear elastic solution and test data using a plot of maximum surface strain in compression and tension versus applied force. The model accounts for damage evolution due to tensile loading and neglects any damage evolution in compression, where the material has higher strength. Simulation and test results are in very good agreement regarding the slope of the load–strain curve and the slope change.

KEY WORDS: short fibre composites; viscoelasticity; damage mechanics; finite element analysis; strength

INTRODUCTION

Models describing mechanical behaviour of polymer matrix composites reinforced with short fibre bundles have to account for viscoelasticity of the resin and microdamage development in form of local matrix cracks. The state of damage is very complex and a development of micro mechanism-based damage models is a complex work for a future. Since the quantification of microdamage entities belonging to different damage modes (matrix cracks in

*Correspondence to: M. Oldenbo, Volvo Car Corporation, Exterior Engineering, Dept 93610, PV3C2, SE-405 31 Göteborg, Sweden.
†E-mail: moldenbo@volvocars.com

Contract/grant sponsor: Volvo Car Corporation
Contract/grant sponsor: VINNOVA; contract/grant number: 2002-01578

Received 17 May 2004
Revised 4 March 2005
Accepted 4 April 2005

bundles, delamination of bundles, matrix cracks outside bundles, fibre cracks in bundles, etc.) and the description of their effect on stiffness is very difficult, a thermodynamics-based approach with internal state variables to describe the damage state is preferred in this paper.

Viscoelastic-damageable material models for short fibre composites scarcely exist in the literature. An example of this kind of model applied to swirl-mat composite is the model by Weitsman [1] who used a power law to describe viscoelasticity and a scaling factor, for damage to model unidirectional creep. Kumar and Talreja [2] have introduced a pseudo-strain energy defined in the Laplace domain to describe viscoelasticity of laminates with different degrees of damage. Hinterhoelzl [3] has implemented a linear viscoelastic-isotropic damage model for reinforced plastics in the FE-program ABAQUS. Fitoussi *et al.* [4] and Guo *et al.* [5] have presented an elastic-damageable material model based on a statistical failure criterion for the identified failure mechanism of interfacial shear failure. This model was implemented in ABAQUS and applied to simple structures. Zocher *et al.* [6] have made a general incremental formulation suitable for orthotropic viscoelasticity. In ABAQUS Standard, a user-defined material model requires an incremental procedure defined in a subroutine, and the frame for this subroutine is given in the option of subroutine UMAT. At the end of the increment for which it is called, UMAT must update stresses and any solution-dependent state variables used. It must also provide the Jacobian matrix, $\partial\Delta\sigma/\partial\Delta\varepsilon$, for the constitutive model.

The non-linear constitutive model for short fibre composite developed by Oldenbo and Varna [7], which accounts for viscoelastic effects and microdamage is used in this paper. The model considers the material as initially in-plane linear viscoelastic and with orthotropic damage development. The continuum damage mechanics theory by Chow and Wang [8] is utilized. A low-density sheet-moulding compound (SMC) composite material containing toughening additive characterized in previous studies, see References [9, 10], is used to demonstrate the potential of the model and the incremental formulation developed below.

The approach is based on the assumption that damage and viscoelastic effects may be separated, that is, damage development is considered as an elastic process and the reduced stiffness due to damage is used as a scaling factor of the linear viscoelastic response. Hence, the time dependence in the damage evolution is neglected which obviously may be a rather rough simplification for certain classes of materials. The relaxation functions of the damaged composite are represented by a product of two terms representing damage and viscoelasticity, respectively. The used assumptions, which are discussed in more details in Reference [7], can be summarized as follows:

- The damage evolution is time independent and is characterized by two damage parameters determined using the measured stiffness reduction in tensile tests.
- Each damage parameter depends only on the corresponding thermodynamic force which means that the material develops cracks only transverse to the applied load in tension.
- Damage evolution in shear- and compression loading is much less than in tensile loading and may be neglected.
- Creep data for undamaged specimens give the time dependence of the non-linear viscoelastic model.

These assumptions simplify the model to a reasonable complexity and suggest a simple methodology for experimental identification of parameters. The validity of the model for SMC

composites has been demonstrated in unidirectional creep tests of samples with different degree of damage and in analytical modelling of tensile loading–unloading tests with different strain rates [7].

The objective of the present paper is to generalize the non-linear one-dimensional model developed previously [7] to the 2D case and to derive an incremental formulation suitable for FE-simulations using shell theory. It is implemented in a commercial FE-solver and is validated simulating (a) constant strain rate tensile test and comparing with an analytical solution; (b) four-point bending test and comparing with experimental data.

2D MATERIAL MODEL FOR FINITE ELEMENT APPLICATIONS

In this paper we are not using the convention that repeating indexes mean summation.

2D formulation of the model

The stress–strain relationship for in-plane components of a linear viscoelastic-damageable material is

$$\sigma_i(t, D) = \sum_j \int_0^t \tilde{C}_{ij}(t-\tau, D)\,\frac{\mathrm{d}\varepsilon_j}{\mathrm{d}\tau}\,\mathrm{d}\tau, \quad i, j = 1, 2, 6 \tag{1}$$

Here D denotes the damage parameters D_1 and D_2 and $\tilde{C}_{ij}(t, D)$ is the damage-reduced relaxation matrix for the case of plane stress:

$$\tilde{C}(t, D) = \begin{bmatrix} \tilde{C}_{11}(t, D) & \tilde{C}_{12}(t, D) & 0 \\ \tilde{C}_{12}(t, D) & \tilde{C}_{22}(t, D) & 0 \\ 0 & 0 & \tilde{C}_{66}(t, D) \end{bmatrix} \tag{2}$$

The relation between damage parameters and the relaxation matrix is taken from the continuum damage mechanics model [8]:

$$[\tilde{C}(t, D)] = [M][C(t)][M]^{\mathrm{T}, -1} \tag{3}$$

where $C_{ij}(t)$ is the relaxation modulus matrix of an undamaged material and $[M]$ is the damage effect tensor:

$$M_{ij} = \begin{bmatrix} \dfrac{1}{1-D_1} & 0 & 0 \\ & \dfrac{1}{1-D_2} & 0 \\ \text{sym} & & \dfrac{1}{\sqrt{(1-D_1)(1-D_2)}} \end{bmatrix} \tag{4}$$

After matrix multiplication $\tilde{C}_{ij}(t)$ may be written explicitly:

$$\tilde{C}_{ij}(t, D) = \begin{bmatrix} (1-D_1)^2 C_{11}(t) & (1-D_1)(1-D_2)C_{12}(t) & 0 \\ (1-D_1)(1-D_2)C_{12}(t) & (1-D_2)^2 C_{22}(t) & 0 \\ 0 & 0 & (1-D_1)(1-D_2)C_{66}(t) \end{bmatrix} \tag{5}$$

Since damage evolution is assumed to be an elastic process the damage state depends only on the maximum (most severe) stress state $\bar{\sigma}(\varepsilon_k(t))$ or strain state $\bar{\varepsilon}(\varepsilon_k(t))$ experienced during the whole service life until the current instant t. The meaning of the 'most severe' will be defined later.

$$D_j = D_j(\bar{\varepsilon}), \quad j = 1, 2 \tag{6}$$

$\tilde{C}_{ij}$ in the stress–strain relationship equation (1) may be written according to Equation (5) as

$$\tilde{C}_{ij}(t, D) = a_i(D) a_j(D) C_{ij}(t) \tag{7}$$

with

$$a_i = \begin{bmatrix} 1-D_1 \\ 1-D_2 \\ \sqrt{(1-D_1)(1-D_2)} \end{bmatrix} \tag{8}$$

Since $D = D(\bar{\varepsilon})$, where $\bar{\varepsilon}$ represents the most severe strain state experienced by the composite during its life, functions a_i are also $a_i(\bar{\varepsilon})$.

Denote

$$b_{ij}(\bar{\varepsilon}) = a_i(\bar{\varepsilon}) a_j(\bar{\varepsilon}) \tag{9}$$

According to Equations (7) and (9), $\tilde{C}_{ij}(t, D)$ may be written as

$$\tilde{C}_{ij}(t, D) = b_{ij}(\bar{\varepsilon}) C_{ij}(t) \quad \text{(no summation over repeating index)} \tag{10}$$

Substituting Equation (10) in Equation (1) we obtain

$$\sigma_i(t, D) = \sum_j b_{ij}(\bar{\varepsilon}) \int_0^t C_{ij}(t-\tau) \frac{\mathrm{d}\varepsilon_j}{\mathrm{d}\tau} \, \mathrm{d}\tau \tag{11}$$

$\bar{\varepsilon}$ can be considered as a complex function of the current strain state ε_l. Hence b_{ij} are monotonously increasing and are also functions of ε_l which change values only if the current strain state is more severe than the worst situation before.

The relaxation functions of the undamaged composite are approximated with a Prony series as

$$C_{ij}(t) = C_{ij}^{\infty} + \sum_m C_{ij}^m \mathrm{e}^{-t/\tau_m} \tag{12}$$

Incremental formulation of the constitutive equations

The presented method is an extension of Reference [6] to also include damage. Now denote $\varepsilon_i^k = \varepsilon_i(t_k)$, $\sigma_i^k = \sigma_i(t_k)$ and introduce:

$$\begin{aligned} t_{k+1} &= t_k + \Delta t \\ \Delta\varepsilon_i(t_k) &= \varepsilon_i^{k+1} - \varepsilon_i^k \\ \Delta\sigma_i(t_k) &= \sigma_i^{k+1} - \sigma_i^k \\ b_{ij}^k &= b_{ij}(\varepsilon_l^k) \end{aligned} \tag{13}$$

According to (11) for $t = t_{k+1}$

$$\begin{aligned} \sigma_i^{k+1} &= \sum_j b_{ij}(\varepsilon_l^{k+1}) \int_0^{t+\Delta t} C_{ij}(t + \Delta t - \tau) \frac{\mathrm{d}\varepsilon_j}{\mathrm{d}\tau}\,\mathrm{d}\tau \\ &= \sum_j b_{ij}(\varepsilon_l^{k+1}) \int_0^{t_k} C_{ij}(t_k + \Delta t - \tau) \frac{\mathrm{d}\varepsilon_j}{\mathrm{d}\tau}\,\mathrm{d}\tau \\ &\quad + \sum_j b_{ij}(\varepsilon_l^{k+1}) \int_{t_k}^{t_{k+1}} C_{ij}(t_k + \Delta t - \tau) \frac{\mathrm{d}\varepsilon_j}{\mathrm{d}\tau}\,\mathrm{d}\tau \end{aligned} \tag{14}$$

and

$$\sigma_i^k = \sum_j b_{ij}(\varepsilon_l^k) \int_0^{t_k} C_{ij}(t_k - \tau) \frac{\mathrm{d}\varepsilon_j}{\mathrm{d}\tau}\,\mathrm{d}\tau \tag{15}$$

Using Equations (14) and (15) in the definition of $\Delta\sigma_i(t_k)$, see Equation (13), gives

$$\begin{aligned} \Delta\sigma_i(t_k) &= \sum_j b_{ij}(\varepsilon_l^{k+1}) \int_0^{t_k} C_{ij}(t_k + \Delta t - \tau) \frac{\mathrm{d}\varepsilon_j}{\mathrm{d}\tau}\,\mathrm{d}\tau - \sum_j b_{ij}(\varepsilon_l^k) \int_0^{t_k} C_{ij}(t_k - \tau) \frac{\mathrm{d}\varepsilon_j}{\mathrm{d}\tau}\,\mathrm{d}\tau \\ &\quad + \sum_j b_{ij}(\varepsilon_l^{k+1}) \int_{t_k}^{t_k+\Delta t} C_{ij}(t_k + \Delta t - \tau) \frac{\mathrm{d}\varepsilon_j}{\mathrm{d}\tau}\,\mathrm{d}\tau \end{aligned} \tag{16}$$

We use a linear approximation

$$b_{ij}(\varepsilon_l^{k+1}) = b_{ij}(\varepsilon_l^k) + \sum_l \left.\frac{\partial b_{ij}}{\partial \varepsilon_l}\right|_{\varepsilon_l^k} \Delta\varepsilon_l(t_k) \tag{17}$$

Denote

$$R_{ijl}^k = \left.\frac{\partial b_{ij}}{\partial \varepsilon_l}\right|_{\varepsilon_l = \varepsilon_l^k} \tag{18}$$

$$b_{ij}^{k+1} = b_{ij}^k + \sum_l R_{ilj}^k \Delta\varepsilon_l(t_k) \tag{19}$$

Substitute Equation (19) in Equation (16)

$$\Rightarrow \Delta\sigma_i(t_k) = \sum_j b_{ij}^k \underbrace{\int_0^{t_k} [C_{ij}(t_k + \Delta t - \tau) - C_{ij}(t_k - \tau)] \frac{\mathrm{d}\varepsilon_j}{\mathrm{d}\tau}\,\mathrm{d}\tau}_{I_1}$$

$$+ \sum_j \left\{ \sum_l R_{ijl}^k \Delta\varepsilon_l(t_k) \right\} \underbrace{\int_0^{t_k} C_{ij}(t_k + \Delta t - \tau) \frac{\mathrm{d}\varepsilon_j}{\mathrm{d}\tau}\,\mathrm{d}\tau}_{I_2}$$

$$+ \sum_j \left\{ b_{ij}^k + \sum_l R_{ijl}^k \Delta\varepsilon_l(t_k) \right\} \underbrace{\int_{t_k}^{t_k+\Delta t} C_{ij}(t_k + \Delta t - \tau) \frac{\mathrm{d}\varepsilon_j}{\mathrm{d}\tau}\,\mathrm{d}\tau}_{I_3} \tag{20}$$

We analyse the integrals I_1, I_2 *and* I_3 *in* (20). I_1 may be written as

$$I_1 = \sum_m [\mathrm{e}^{-\Delta t/\tau_m} - 1] \int_0^{t_k} C_{ij}^m \mathrm{e}^{-(t_k-\tau)/\tau_m} \frac{\mathrm{d}\varepsilon_j}{\mathrm{d}\tau}\,\mathrm{d}\tau \tag{21}$$

Define

$$\sigma_{ij}^m(t) = \int_0^t C_{ij}^m \mathrm{e}^{-(t-\tau)/\tau_m} \frac{\mathrm{d}\varepsilon_j}{\mathrm{d}\tau}\,\mathrm{d}\tau \tag{22}$$

Equation (21) becomes

$$I_1 = \sum_m [\mathrm{e}^{-\Delta t/\tau_m} - 1] \sigma_{ij}^m(t_k) \tag{23}$$

Now the first term in Equation (20) can be rewritten and denoted as $\Delta\sigma_i^R$:

$$\Delta\sigma_i^R(t_k) = -\sum_j b_{ij}^k \sum_m (1 - \mathrm{e}^{-\Delta t/\tau_m}) \sigma_{ij}^m(t_k) \tag{24}$$

It can be shown, see Reference [6], that the following recursive expression may be used to calculate $\sigma_{ij}^m(t_k)$:

$$\sigma_{ij}^m(t_k) = \mathrm{e}^{-\Delta t/\tau_m} \sigma_{ij}^m(t_{k-1}) + (1 - \mathrm{e}^{-\Delta t/\tau_m}) C_{ij}^m \frac{\tau_m}{\Delta t} \Delta\varepsilon_j^{k-1} \tag{25}$$

Consider $I_2 = \int_0^{t_k} C_{ij}(t_k + \Delta t - \tau)(\mathrm{d}\varepsilon_j/\mathrm{d}\tau)\,\mathrm{d}\tau$ *in Equation* (20). Substitute Equation (12) in expression for I_2 to obtain

$$I_2 = C_{ij}^\infty \varepsilon_j^k + \sum_m \mathrm{e}^{-\Delta t/\tau_m} \int_0^{t_k} C_{ij}^m \mathrm{e}^{-(t_k-\tau)/\tau_m} \frac{\mathrm{d}\varepsilon_j}{\mathrm{d}\tau}\,\mathrm{d}\tau \tag{26}$$

Equation (26) may be written as

$$I_2 = C_{ij}^\infty \varepsilon_j^k + \sum_m \mathrm{e}^{-\Delta t/\tau_m} \sigma_{ij}^m(t_k) \tag{27}$$

Consider $I_3 = \int_{t_k}^{t_k+\Delta t} C_{ij}(t_k + \Delta t - \tau)(\mathrm{d}\varepsilon_j/\mathrm{d}\tau)\,\mathrm{d}\tau$ *in Equation* (20). Substitute Equation (12) in expression for I_3 to obtain

$$I_3 = \int_{t_k}^{t_k+\Delta t} C_{ij}^{\infty} + \sum_m C_{ij}^m \mathrm{e}^{-(t_k+\Delta t-\tau)/\tau_m} \frac{\mathrm{d}\varepsilon_j}{\mathrm{d}\tau}\,\mathrm{d}\tau \tag{28}$$

Presenting ε_j in interval $t_k \leqslant t \leqslant t_{k+1}$ in linearized form:

$$\varepsilon_j(\tau) = \varepsilon_j(t_k) + R_j^{\varepsilon}(t-\tau)H(\tau - t_k) \tag{29}$$

where

$$R_j^{\varepsilon} = \left.\frac{\mathrm{d}\varepsilon_j}{\mathrm{d}t}\right|_{t=t_k} = \left.\frac{\Delta\varepsilon_j}{\Delta t}\right|_{t=t_k} \tag{30}$$

we have

$$\frac{\mathrm{d}}{\mathrm{d}\tau}\{\varepsilon_j(\tau)\} = R_j^{\varepsilon}H(\tau - t_k) + R_j^{\varepsilon}(\tau - t_k)\delta(\tau - t_k) \tag{31}$$

Substituting Equation (31) in Equation (28)

$$\begin{aligned}
\Rightarrow I_3 &= C_{ij}^{\infty} R_j^{\varepsilon}\Delta t + \sum_m C_{ij}^m \int_{t_k}^{t_k+\Delta t} \mathrm{e}^{-(t_k+\Delta t-\tau)/\tau_m} R_j^{\varepsilon}\,\mathrm{d}\tau \\
&= C_{ij}^{\infty}\Delta\varepsilon_j(t_k) + \sum_m C_{ij}^m \tau_m \int_{-\Delta t/\tau_m}^{0} \mathrm{e}^u R_j^{\varepsilon}\,\mathrm{d}u \\
&= \left\{C_{ij}^{\infty} + \sum_m C_{ij}^m \frac{\tau_m}{\Delta t}(1 - \mathrm{e}^{-\Delta t/\tau_m})\right\}\Delta\varepsilon_j(t_k)
\end{aligned} \tag{32}$$

The third term in Equation (20) now is

$$\sum_j \left\{b_{ij}^k + \sum_l R_{ijl}^k \Delta\varepsilon_l(t_k)\right\}\left[C_{ij}^{\infty} + \sum_m C_{ij}^m \frac{\tau_m}{\Delta t}(1 - \mathrm{e}^{-\Delta t/\tau_m})\right]\Delta\varepsilon_j(t_k) \tag{33}$$

(keeping only linear term with respect to $\Delta\varepsilon_j$, i.e. neglecting $\Delta\varepsilon_l \cdot \Delta\varepsilon_j$)

$$= \sum_j b_{ij}^k \left[C_{ij}^{\infty} + \sum_m C_{ij}^m \frac{\tau_m}{\Delta t}(1 - \mathrm{e}^{-\Delta t/\tau_m})\right]\Delta\varepsilon_j(t_k) \tag{34}$$

Using Equations (23), (24), (27) and (33), (34) it is possible to write Equation (20) as

$$\begin{aligned}
\Delta\sigma_i(t_k) = \Delta\sigma_i^R(t_k) &+ \sum_j \left\{\sum_l R_{ijl}^k \Delta\varepsilon_l(t_k)\right\}\left[C_{ij}^{\infty}\varepsilon_j^k + \sum_m \mathrm{e}^{-\Delta t/\tau_m}\sigma_{ij}^m(t_k)\right] \\
&+ \sum_j b_{ij}^k \left[C_{ij}^{\infty} + \sum_m C_{ij}^m \frac{\tau_m}{\Delta t}(1 - \mathrm{e}^{-\Delta t/\tau_m})\right]\Delta\varepsilon_j(t_k)
\end{aligned} \tag{35}$$

Changing the sequence of summation in the second term of Equation (35) gives

$$\Delta\sigma_i(t_k) = \Delta\sigma_i^R(t_k) + \sum_j \left\{ \sum_l R_{ilj}^k \left[C_{il}^\infty \varepsilon_l^k + \sum_m \mathrm{e}^{-\Delta t/\tau_m} \sigma_{il}^m(t_k) \right] \right\} \Delta\varepsilon_j(t_k)$$
$$+ \sum_j b_{ij}^k \left[C_{ij}^\infty + \sum_m C_{ij}^m \frac{\tau_m}{\Delta t}(1 - \mathrm{e}^{-\Delta t/\tau_m}) \right] \Delta\varepsilon_j(t_k) \tag{36}$$

With

$$R_{ilj}(t_k) = \left. \frac{\partial b_{il}}{\partial \varepsilon_j} \right|_{t=t_k} \tag{37}$$

Denote

$$\hat{C}_{ij} = b_{ij}^k \left[C_{ij}^\infty + \sum_m C_{ij}^m \frac{\tau_m}{\Delta t}(1 - \mathrm{e}^{-\Delta t/\tau_m}) \right] \tag{38}$$

$$\hat{\Gamma}_{ij} = \sum_l R_{ilj}^k \left[C_{il}^\infty \varepsilon_l^k + \sum_m \mathrm{e}^{-\Delta t/\tau_m} \sigma_{il}^m(t_k) \right] \tag{39}$$

and

$$\hat{Q}_{ij} = \hat{C}_{ij} + \hat{\Gamma}_{ij} \tag{40}$$

The final form of the incremental constitutive law is

$$\Delta\sigma_i(t_k) = \sum_j \hat{Q}_{ij}(t_k) \Delta\varepsilon_j(t_k) + \Delta\sigma_i^R(t_k) \tag{41}$$

Determination of damage parameters for the current stress state

In a thermodynamics approach the damage evolution is governed by associated thermodynamic forces. The thermodynamic force Y_i, associated with a certain damage variable D_i, may be found using the expression for strain energy Ψ^e of the damaged composite and taking derivatives with respect to this variable:

$$Y_i = \frac{\partial \Psi^e}{\partial D_i} \tag{42}$$

Ψ^e is calculated based on the definition of the strain energy:

$$\Psi^e = \frac{1}{2} \sum_i \sum_j \sigma_{ij} \varepsilon_{ij} \tag{43}$$

and the result is

$$\Psi^e = \frac{\sigma_1^2 C_{22}}{2(1-D_1)^2(C_{22}C_{11}-C_{12}^2)} + \frac{\sigma_2^2 C_{11}}{2(1-D_2)^2(C_{22}C_{11}-C_{12}^2)} - \frac{\sigma_1\sigma_2 C_{12}}{(1-D_1)(1-D_2)(C_{22}C_{11}-C_{12}^2)} + \frac{\sigma_6^2}{2(1-D_1)(1-D_2)C_{66}} \tag{44}$$

The derivatives with respect to the damage parameters are found to be

$$Y_1 = \frac{\partial \Psi^e}{\partial D_1} = \frac{\sigma_1^2 C_{22}}{(1-D_1)^3(C_{22}C_{11}-C_{12}^2)} - \frac{\sigma_1\sigma_2 C_{12}}{(1-D_1)^2(1-D_2)(C_{22}C_{11}-C_{12}^2)} + \frac{\sigma_6^2}{2(1-D_1)^2(1-D_2)C_{66}} \tag{45}$$

$$Y_2 = \frac{\partial \Psi^e}{\partial D_2} = \frac{\sigma_2^2 C_{11}}{(1-D_2)^3(C_{22}C_{11}-C_{12}^2)} - \frac{\sigma_1\sigma_2 C_{12}}{(1-D_1)(1-D_2)^2(C_{22}C_{11}-C_{12}^2)} + \frac{\sigma_6^2}{2(1-D_1)(1-D_2)^2C_{66}} \tag{46}$$

The evolution law is formulated if the dependence of damage variables on thermodynamic forces is defined. The value of a damage variable cannot decrease which means that it is not a function of the current stress state but it is a function of the most severe stress state before or in the current instant of time, or more exactly, it depends on the thermodynamic force in this stress state. This value of the thermodynamic forces is denoted $Y_i = \bar{Y}_i$

$$\begin{aligned} D_1 &= f_1(\bar{Y}_1, \bar{Y}_2) \\ D_2 &= f_2(\bar{Y}_1, \bar{Y}_2) \end{aligned} \tag{47}$$

Obviously in a new stress state characterized by a different combination of Y_1 and Y_2 the damage will grow only if the values of f_1 and f_2 are higher than in the previous most severe stress state. In a general loading case, both damage variables are functions of both associated forces and identification of these functions using test data is not trivial. If damage parameters are assumed uncoupled the simplified relations are

$$\begin{aligned} D_1 &= f_1(\bar{Y}_1) \\ D_2 &= f_2(\bar{Y}_2) \end{aligned} \tag{48}$$

If the material is assumed initially planar isotropic the relations in Equation (47) are fully analogous, i.e. if the relation $D_1 = f_1(\bar{Y}_1, \bar{Y}_2)$ is known, $D_2 = f_2(\bar{Y}_1, \bar{Y}_2)$ is known as well. Equation (47) must be obtained experimentally and in previous work [7, 11] it has been shown

that, using uniaxial tensile loading data, an initially isotropic short fibre composite can be described with a linear relationship:

$$\begin{aligned} D_1 &= a(\bar{Y}_1 - Y_0) \\ D_2 &= 0 \end{aligned} \tag{49}$$

where a and Y_0 are constants.

$D_2 \neq f_2(\bar{Y}_1)$ validates the simplification made in Equation (48) for the case where only one thermodynamic force is non-zero and value of $\bar{Y}_1$ is moderate. For the most severe strain state, $\bar{\varepsilon}(\varepsilon_k(t))$, experienced by the material, Equations (45) for D_1, respectively, (46) for D_2 have to be solved with Equation (49) in an iterative manner. This is done, for example, using Newton–Raphson iterations. In the general Newton–Raphson iteration equation

$$D_1^{n+1} = D_1^n - \frac{f(D_1)}{f'(D_1)} \tag{50}$$

$f(D_1)$ is obtained by eliminating Y_1 from $Y_1 = \partial\Psi^e/\partial D_1$ in Equation (45) by using $D_1(Y_1)$ in Equation (49). The result is

$$\begin{aligned} f(D_1) = (D_1 + aY_0)(1 - D_1)^3 - \frac{a\sigma_6^2(1 - D_1)}{2(1 - D_2)C_{66}(t)} + \frac{a\sigma_1\sigma_2 C_{12}(t)(1 - D_1)}{(1 - D_2)(C_{22}(t)C_{11}(t) - C_{12}^2(t))} \\ - \frac{a\sigma_1^2 C_{22}(t)}{C_{22}(t)C_{11}(t) - C_{12}^2(t)} \end{aligned} \tag{51}$$

$f'(D_1)$ is easily found since

$$f'(D_1) = \frac{\partial f(D_1)}{\partial D_1} \tag{52}$$

Since theoretically four different roots are possible, an understanding of the sensitivity to a correct starting point is found by plotting $f(D_1)$ in the region $0 \leqslant D_1 \leqslant 1$. For an initially in-plane isotropic material, updating of damage parameter D_2 is analogous to updating of D_1 shown here. D_2 which according to Equation (51) is needed in calculation of D_1, is taken from the previous time step.

IMPLEMENTATION IN FE-SOLVER

Material data are the relaxation stiffness matrix of an undamaged composite described with Prony series and the damage development law in Equation (49). The relaxation stiffness matrix components are calculated from $E(t)$ and $v(t)$ considering the undamaged material as in-plane

isotropic [12]:

$$\begin{aligned} C_{11}(t) &= \frac{E(t)}{1-\nu(t)^2} \\ C_{22}(t) &= C_{11}(t) \\ C_{12}(t) &= \frac{\nu(t)E(t)}{1-\nu(t)^2} \\ C_{66}(t) &= \frac{E(t)}{2(1+\nu(t))} \end{aligned} \tag{53}$$

The relaxation stiffness matrix, in form of relaxation times and coefficients in the Prony series (see in Equation (12)), are put directly in the FE-solver ABAQUS input file which includes geometry, load case and description of the FE-analysis to be performed. Transverse shear stiffness required in ABAQUS is given as a constant calculated from the out-of-plane shear relaxation stiffness, G_{13}, for linear elastic orthotropic material [13]:

$$K_{11} = K_{22} = \tfrac{5}{6} G_{13} h \tag{54}$$

Here h is the thickness of the shell.

The material model is implemented in the UMAT subroutine for user-defined material models. The subroutine updates stress and tangential stiffness, i.e. Jacobian, for the next increment. Introduction of the damage tensor $b_{ij}(\bar{\varepsilon})$ leads to a scaling parameter to the viscoelastic solution, see Equations (24), (38) and (39). To solve Equation (37) for $R_{ilj}(t_k)$ where the derivatives of $b_{ij}(\bar{\varepsilon})$ for all strains are needed we use finite differences:

$$R_{ilj}(t_k) = \frac{\Delta b_{il}}{\Delta \varepsilon_j} \tag{55}$$

with

$$\begin{aligned} \Delta b_{il} &= b_{il}(t_k) - b_{il}(t_{k-1}) \\ \Delta \varepsilon_j &= \varepsilon_j(t_k) - \varepsilon_j(t_{k-1}) \end{aligned} \tag{56}$$

Damage data and strain increments needed to calculate Equation (56) are stored as solution-dependent state variables (SDSV). $\sigma_{ij}^m(t_k)$ in Equation (25) is solved in a recursive manner and $\sigma_{ij}^m(t_{k-1})$ is also stored as SDSV. The Jacobian used to balance internal and external forces is

$$J = \hat{Q}_{ij} = \hat{C}_{ij} + \hat{\Gamma}_{ij} \tag{57}$$

The damage parameters are updated after updating the stress. This means that D_{k-1} is used at t_k instead of D_k. Using D_k is possible on expense of calculation time using iterations to correlate updated damage state with updated stress state. However, if increments are sufficiently small, it gives only a little improvement of the result. Cracks in the material develop transverse to the applied load and the first principal stress determines the direction of the main damage level. A local coordinate system coinciding with the principal stress directions is obtained from the initial increment of strain, assuming that the change in rotations of microcracks stay small during the rest of the simulation, see Reference [3]. The obtained D_1, which corresponds

to damage in the material direction with most damage, can be compared with an acceptable damage level, however the determination of a acceptable damage level is out of the scope of this work.

VERIFICATION OF ABAQUS IMPLEMENTATION

Material data

The SMC composite used in simulations described below exhibits time-dependent behaviour illustrated in Figure 1. The slope of the stress–strain curve in tensile loading depends on

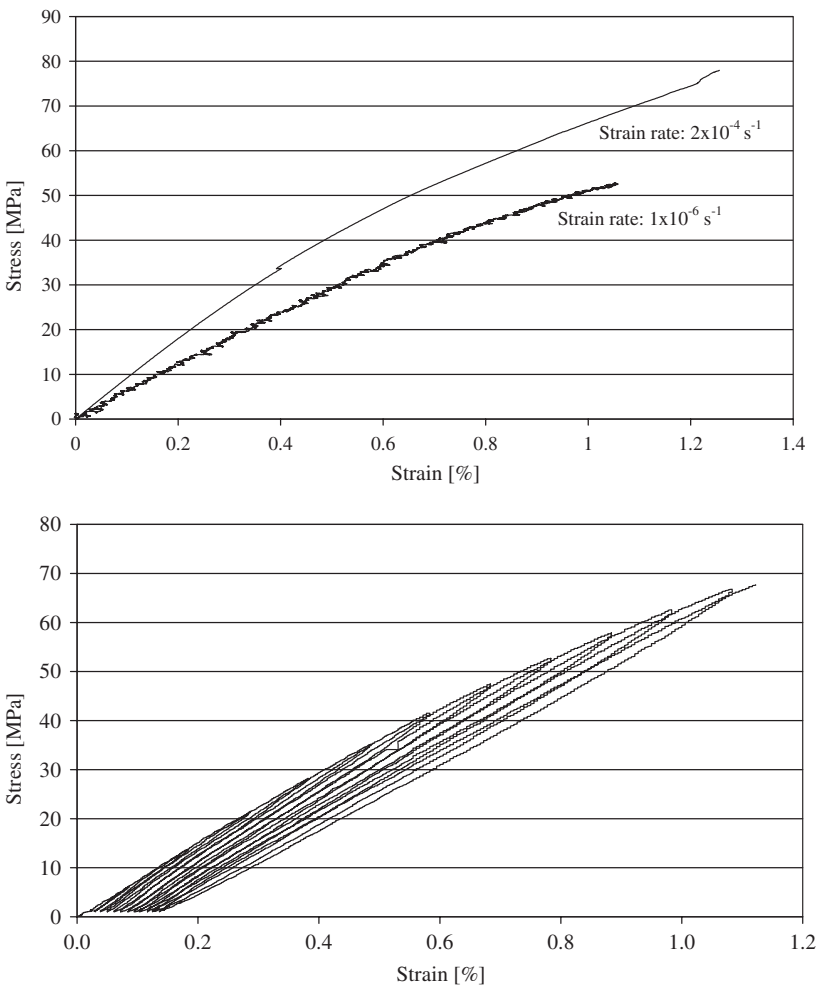

Figure 1. Time dependence of SMC composite with toughening and low-density additives. (Above) A typical stress–strain tensile loading curve at two strain rates is seen and (below) hysteresis in cyclic loading–unloading curve with increasing maximum strain per cycle can be seen.

the strain rate, see Figure 1 (above). Hystheresis loops and slope reduction are observed in tensile loading and unloading tests with increasing maximum strain, see Figure 1 (below). As it was demonstrated in Reference [7] the material model with the assumptions formulated in the Introduction section gives rather good approximation of the tensile test, slightly overestimating the non-linearity for high strain rates and underestimating it for slow strain rates. The reason for discrepancies is believed to be the time-dependent damage development which is not included in the model. The relaxation functions $E(t)$ and $v(t)$ are calculated point by point using the quasi-elastic approach and uniaxial creep data from Reference [7]. The calculated $E(t)$ and $v(t)$ curves are seen in Figure 2. The Poisson's ratio is decreasing during the first 100 s and then stabilizing. A possible reason for this behaviour is an initially not perfectly uniaxial stress field in the test specimen due to presence of clamped ends. It might be better to use the asymptotic value in calculations but at this point it was decided to use the unmodified data. The resulting relaxation matrix components are seen in Figure 3 together with the transverse shear relaxation moduli (see below). The corresponding Prony series, see Equation (8), coefficients and relaxation times based on these curves are seen in Table I.

Equation (49) was obtained experimentally for an SMC composite in a previous work [7] based on E-modulus measurements in unidirectional tensile test on specimens with different degrees of damage. The results are for $\bar{Y}_2 = 0$ and $\bar{Y}_1 \leqslant 0.5$ MPa:

$$\begin{aligned} D_1 &= a(\bar{Y}_1 - Y_0) \\ D_2 &= 0 \end{aligned} \tag{58}$$

with $a = 0.205\ \text{MPa}^{-1}$ and $Y_0 = 0.0654$ MPa.

For FE-simulation of a geometry modelled with shell theory the out-of-plane shear modulus, $G_{13} = G_{23}$ is needed in addition to Equation (2), see Equation (54). However, its influence is generally small and it may be treated separately in a simplified manner. In simulations a

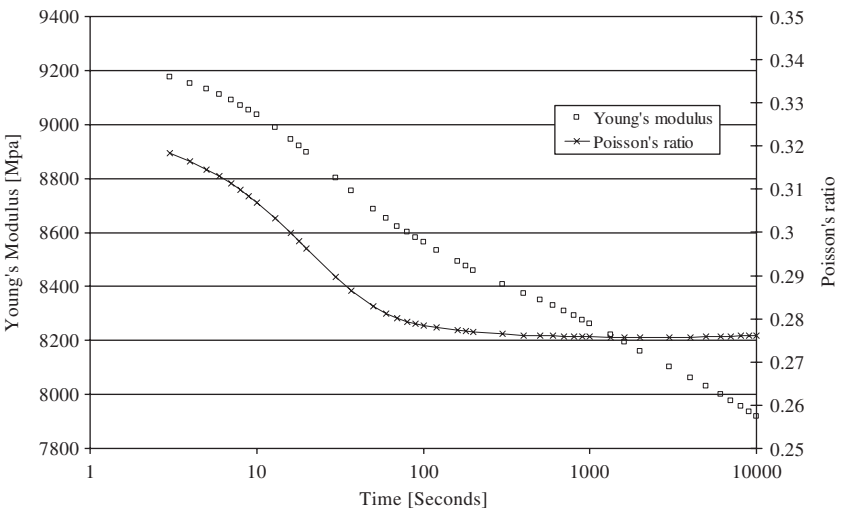

Figure 2. Graph showing evolution of relaxation modulus and Poisson's ratio of undamaged material.

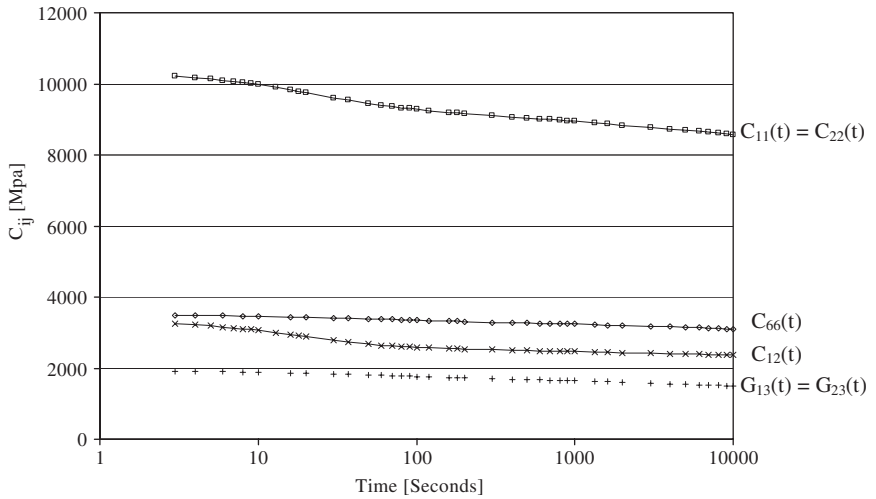

Figure 3. Relaxation stiffness matrix (plane stress assumed) components for undamaged SMC composite with random fibre orientation.

Table I. Prony series relaxation times and coefficients.

Relaxation time	Coefficient	$E(t)$ (MPa)	$\nu(t)$	$C_{11}(t)$ (MPa)	$C_{12}(t)$ (MPa)	$C_{66}(t)$ (MPa)
$\tau_0 = \infty$	C^∞	7751	0.2767	8396	2325	3034
$\tau_1 = 20$	C^1	462	0.0430	795	669	68
$\tau_2 = 100$	C^2	314	0.0049	354	132	111
$\tau_3 = 10^3$	C^3	267	0.0013	301	99	100
$\tau_4 = 10^4$	C^4	457	−0.0015	483	116	185

constant value of G_{13} is used, representing the average value from Figure 3 in the time studied. The shear relaxation modulus $G_{13}(t)$ is calculated using relaxation functions of the matrix and elastic properties of the fibre. Elastic properties of the fibres are given in Reference [14], i.e. Young's modulus 72 GPa and Poisson's ratio 0.22. Properties of the matrix are obtained by inverse modelling and the in-plane creep data for SMC composite are used as input. A micromechanical model by Eduljee *et al.* [15] and Eduljee and McCullough [16] for a hypothetical composite with aligned ellipsoidal inclusions has been used in combination with averaging over fibre orientation distribution described by McCullough *et al.* [17]. See for example Reference [14], for details of the application of this model to SMC composite. For any time instant t, the matrix relaxation functions were calculated using quasi-elastic method as the ones that give the best fit to the composite's in-plane relaxation function. The resulting out-of-plane shear stiffness G_{13} as a function of time is calculated using the same model [14–17] and the result is seen in Figure 3.

Tensile test

In a typical tensile test the loading ramp is unidirectional strain that increases linearly with time:

$$\varepsilon_1 = \dot{\varepsilon} t \tag{59}$$

In Reference [7] a tensile test was performed on the SMC composite at two constant strain rates. The used constant crosshead speed corresponded to (a) strain rate in a standard test following ASTM D3039 and; (b) very low strain rate (a factor 200 lower than the standard test). The strain rates for these tests were 2×10^{-4} and $1.0 \times 10^{-6}\,\mathrm{s}^{-1}$, respectively. In addition, the uniform stress distribution in tensile tests with these strain rates was simulated using an analytic expression based on the non-linear model explained here, see Reference [7]. The model predicted the stress–strain curve with good accuracy until the region close to failure where new mechanisms not accounted for are taking place. Due to time-dependent crack growth not accounted for in the model, slow strain rate failure occurs earlier in reality than in the model predictions. However, the focus in this section is to validate the developed 2D incremental formulation simulating the tensile test with ABAQUS and the UMAT subroutine and comparing with the analytic result in Reference [7].

The FE-model for the tensile test is reduced to a single ABAQUS S4 element. The boundary condition is that the element is locked in 1-direction at one end and a constant strain rate (also in 1-direction) is applied to the opposite end. It is seen in Figure 4 that the FE-result and analytical result coincide for both strain rates. With the used time increments the simplification of using the damage state from previous increment is leading only to a negligible error.

Four-point bending test

A four-point bending test, see Figure 5, has been modelled using an FE-model built from ABAQUS S4 shell elements. The model is seen in Figure 6 together with the deformed shape

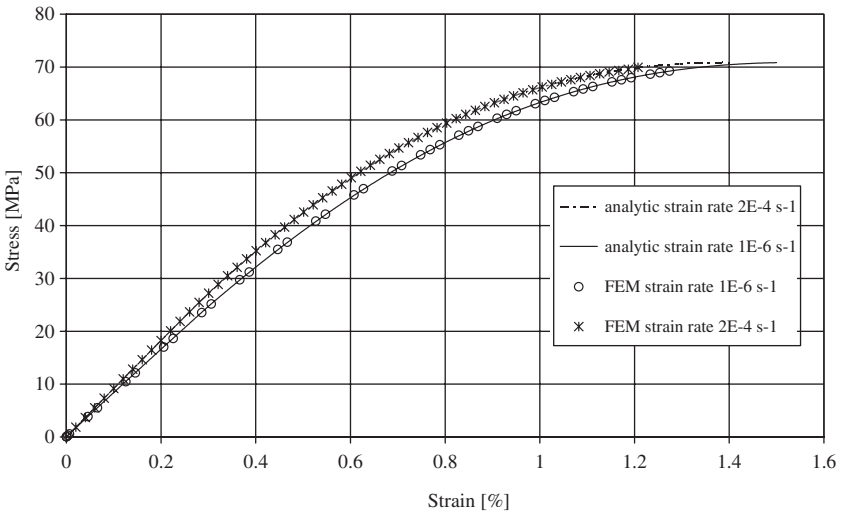

Figure 4. Tensile test—analytic simulation and FE-analysis at two strain rates.

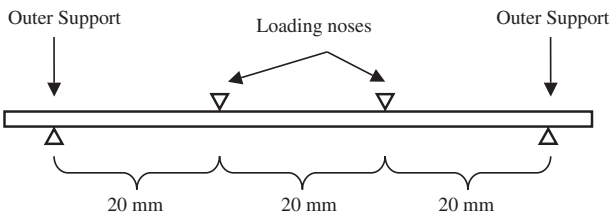

Figure 5. Scheme of the four-point bending test.

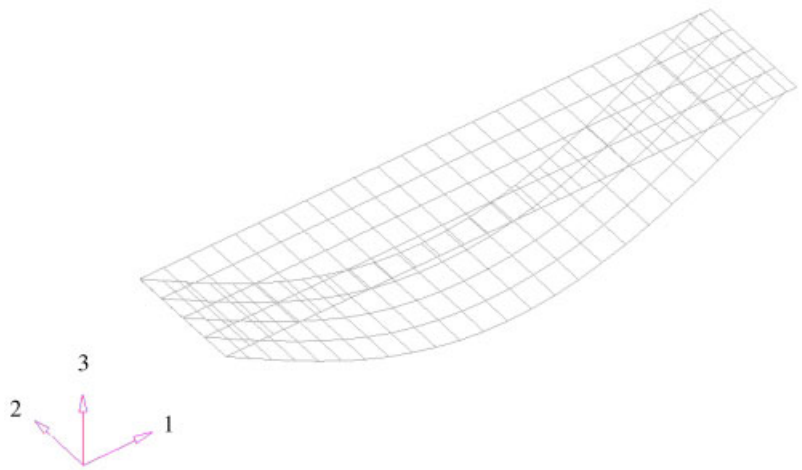

Figure 6. FE-model for bending test specimen and deformed shape (10 times magnified).

at the end of simulation (magnified 10 times). Five integration points through the thickness are used. The model is locked in 3-direction at the ends (at the location of the outer supports) and node forces in negative 3-direction are applied at the location of loading noses. The results are compared with test data and the set-up corresponds to ASTM D6272 for a four-point bending test. According to the standard for a specimen with size $3.025 \times 12.7 \times 75$ mm the support span is 60 mm. The loading rate corresponds to a displacement rate of 2.2 mm/min at the loading noses. Since the damage parameters are uncoupled, damage development in 2D is described with the following relations for D_1 and D_2:

$$\begin{aligned} D_1 &= a(\bar{Y}_1 - Y_0) \\ D_2 &= a(\bar{Y}_2 - Y_0) \end{aligned} \tag{60}$$

where the constants a and Y_0 remains the same as in Equation (58).

The model assumes that there is no damage development due to compression. The reason for the simplification made is that previous research [9, 18] indicates that the compressive strength of SMC is approximately twice the tensile strength. It was not possible to continue the simulation after failure on any surface, limiting the simulation to 1.2% strain (versus an

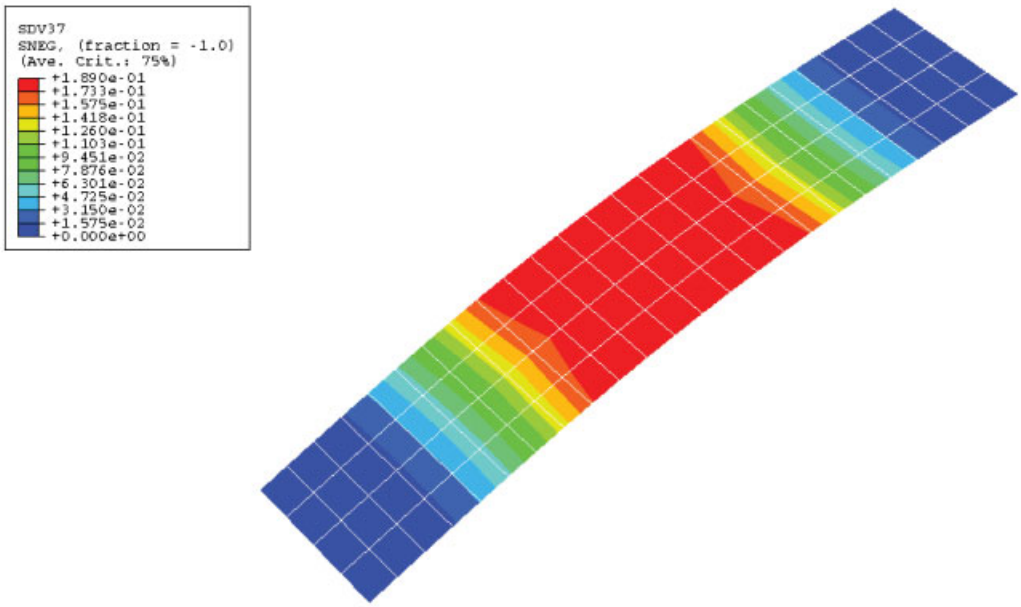

Figure 7. Contour plot from simulation showing damage parameter D_1 on the face in traction.

analytically obtained failure strain of 1.4%). Maximum stress levels at the end of the simulation are found to be 69.9 MPa on the face in traction and 93 MPa on the face in compression. The stress level at the face in traction is in perfect agreement with the tensile test in Figure 4, as would be expected, and there is a very evident difference in stress level at the face in compression compared to at the face in traction. This is due to the fact that there is a substantial damage development in the face in traction but no damage on the part of the specimen that is in compression. In Figure 7, damage parameter D_1 on the face in traction is seen and the maximum value is $D_1 = 0.189$. Due to Poisson's effect we observe saddled surface and the centre of the specimen is buckling towards the applied load. As a result the strain in the 1-direction is higher at the edges and is giving slightly higher damage level (parameter D_1) there. The damage parameter for the direction transverse to the loading, D_2, was found to be zero over the surface in compression indicating that the tensile strain in 2-direction is below the onset of damage development. In Figure 8, a simulation using the model is compared with a simulation using a linear elastic material model with the same initial E-modulus. The strains on the surface in traction, respectively, on the surface in compression in the centre of the specimen are plotted versus the force applied on the loading noses. It is evident that the surface strain level is higher using a non-linear model and the progressive degradation of the material is revealed. Comparison of the simulated strain at surface in traction and compression show that damage leads to more strain at surface in traction than on the other side in agreement with the result for damage previously discussed.

Comparison with the test data is seen in Figure 9. Also in the test the strain on surface in traction is higher than in compression, validating the assumption that damage development in traction is dominant. It is also seen that the slope and magnitude of the simulated and

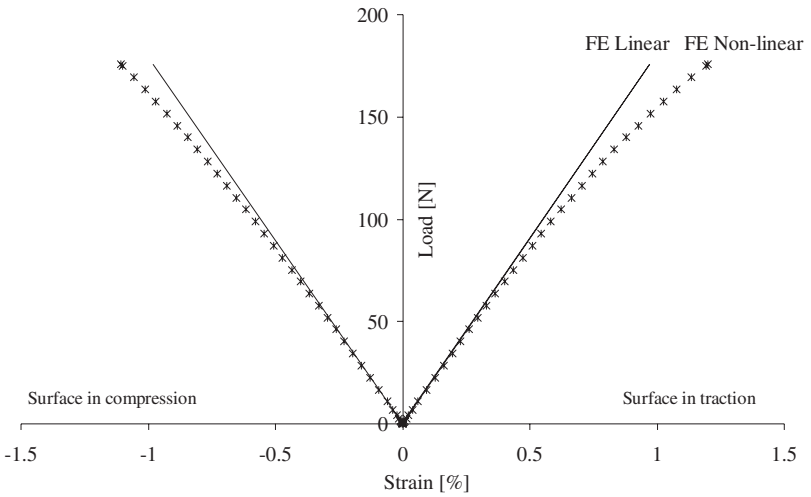

Figure 8. Graph comparing surface strain in the centre of a specimen versus applied force on the loading noses in a simulated bending test, using the developed model and a linear model.

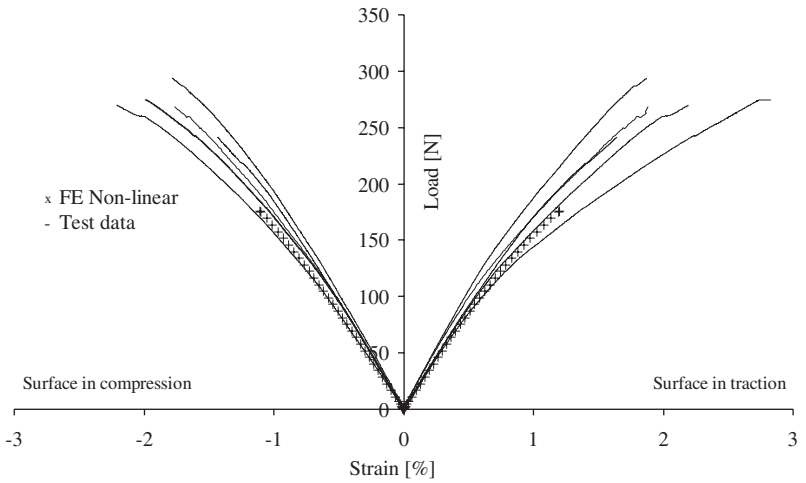

Figure 9. Graph comparing surface strain in centre of specimen versus applied force on the loading noses for simulations and tests (five specimens).

tested response are in good agreement. However, the strain and load at failure in tests are significantly higher than in the simulation ending at 1.2% strain on the surface in traction. In the test, the maximum surface strain is 1.9% on average, with a standard deviation of 0.2% for the five tested samples. Such strain at failure in tension loading is not realistic for this material. The reason for this result is likely that in bending the material's load bearing capacity is not critically dependent on the surface layer failure. The surface, even though severely

damaged, holds together enough to ensure the strain gage function. The specimen sustains load until a critical number of load-bearing bundles is neutralized. From a physical perspective, a neutralized load-bearing bundle in SMC material is a longitudinal fibre bundle that does not carry load, that is, it is broken or interfacially debonded from the matrix. The feature of SMC composite not to fail in bending even though the surface fails is an advantage compared to material sensitive to failure initiations such as most injection-moulded thermoplastics. It would be of interest to study the mechanisms of failure in a bending test from a through the thickness perspective.

CONCLUSIONS

I. A previously developed material model accounting for linear viscoelasticity and damage development in composites was described in incremental formulation. A FORTRAN code is written to implement the model in FE-programme ABAQUS through the option of a user-defined material model written in a subroutine.
II. The incremental formulation was applied to constant strain rate tensile tests on SMC composites and the accuracy of the incremental formulation and the subroutine was proved comparing analytical and FE results. Simulation is possible until strain levels close to the failure when too low tangential stiffness (Jacobian) becomes a numerical issue.
III. Surface strains in bending test at both the face in traction as well as the face in compression are simulated with good accuracy compared to the test data. The simulated surface failure strain is lower than the actual failure strain of the structural part, which indicates that the specimen does not fail at the same time as the surface strain is critical. Apparently, the SMC material is not sensitive to failure initiation.

ACKNOWLEDGEMENTS

The authors wish to thank Dr Magnus Svanberg and Dr Anders Holmberg at the Swedish Institute of Composites (SICOMP AB) for fruitful discussions and assistance. A lot of time was saved using the incremental formulation of orthotropic viscoelasticity by Zocher *et al.* which was already implemented in ABAQUS by SICOMP in an earlier project (see Reference [19]). This work was sponsored by Volvo Car Corporation and VINNOVA in Sweden through the Vehicle Research Program (PFF), Grant No. 2002-01578.

REFERENCES

1. Weitsman YJ. Time-dependent behavior of randomly reinforced polymeric composites. *Mechanics of Composite Materials* 2002; **38**:381–386.
2. Kumar RS, Talreja R. A continuum damage model for linear viscoelastic composite materials. *Mechanics of Materials* 2003; **35**:463–480.
3. Hinterhoelzl RM. Coupling the theory of viscoelasticity and continuum damage mechanics to model the time dependent behavior of fiber reinforced plastics and particulate composites. *International Journal of Materials and Product Technology* 2002; **17**:121–133.
4. Fitoussi J, Guo G, Baptiste D. A statistical micromechanical model of anisotropic damage for SMC composites. *Composites Science and Technology* 1998; **58**:759–763.

5. Guo G, Fitoussi J, Baptiste D. Modelling of damage behaviour of a short-fiber reinforced composite structure by the finite element analysis using a micro-macro law. *International Journal of Damage Mechanics* 1997; **6**:278–299.
6. Zocher MA, Groves SE, Allen DH. A three-dimensional finite element formulation for thermoviscoelastic orthotropic media. *International Journal for Numerical Methods in Engineering* 1997; **40**:2267–2288.
7. Oldenbo M, Varna J. A constitutive model for non-linear behaviour of SMC accounting for linear viscoelasticity and micro damage. *Polymer Composites* 2005; **26**:84–97.
8. Chow CL, Wang J. An anisotropic theory of elasticity for continuum damage mechanics. *International Journal of Fracture* 1987; **33**:3–16.
9. Oldenbo M, Fernberg SP, Berglund LA. Mechanical behavior of SMC composites with toughening and low density additives. *Composites Part A* 2003; **34**:875–885.
10. Fernberg SP, Berglund LA. Bridging law and toughness characterisation of CSM and SMC composites. *Composites Science and Technology* 2002; **61**:2445–2454.
11. Dano ML, Gendron G, Mir H. Mechanics of damage and degradation in random short glass fiber reinforced composites. *Journal of Thermoplastic Composites Materials* 2002; **15**:169–177.
12. Fung YC, Tong P. *Classical and Computational Solid Mechanics*. World Scientific: Singapore, 2001.
13. ABAQUS 6.3-1 Documentation. *Standard User's Manual*. Hibbitt, Karlsson & Sorensen, Inc., 2002.
14. Oldenbo M, Mattsson D, Varna J, Berglund LA. Global stiffness of a SMC panel considering process induced fiber orientation. *Journal of Reinforced Plastics and Composites* 2004; **23**:37–49.
15. Eduljee RF, McCullough RL, Gillespie JW. The influence of inclusion geometry on the elastic properties of discontinuous fiber composites. *Polymer Engineering and Science* 1994; **34**:352–360.
16. Eduljee RF, McCullough RL. *Structures and Properties of Composites*. VCH: New York, 1993; 381–474.
17. McCullough RL, Jarzebski GJ, McGee SH. Constitutive relationships for sheet moulding materials. *Proceedings of a Joint U.S.–Italy Symposium on Composite Materials*, June 15–19, 1981.
18. Taggart DG, Pipes RB, Blake RA, Gillespie Jr JW, Prabhakaran R, Whitney JM. Properties of SMC composites. *Report No. CCM-79-1*, Center for Composite Materials, University of Delaware, Newark, Delaware, 1979.
19. Allen DH, Holmberg JA, Ericson M, Lans L, Svensson N, Holmberg S. Modeling the viscoelastic response of GMT structural components. *Composites Science and Technology* 2001; **61**:503–515.

